JETIR.ORG ISSN: 2349-5162 | ESTD Year : 2014 | Monthly Issue
JOURNAL OF EMERGING TECHNOLOGIES AND INNOVATIVE RESEARCH (JETIR)
An International Scholarly Open Access, Peer-reviewed, Refereed Journal

Photocatalytic Degradation Of Methylene Blue Dye Over Sr Doped $LaCoO_3$ Nano-catalyst Under Sun Light Irradiation

Archana B. Bodade[*1], Anjali B. Bodade[2], G. N. Chaudhari[3], S. M. Ghodsal[4]

1 Department of Physics, Shri Shivaji Science College, Amravati, India.
archanabodade2005@gmail.com
2,3,4. Nano Technology Research Laboratory, Department of Chemistry, Shri Shivaji Science College, Amravati, India.

ABSTRACT

$LaCoO_3$ and $La_{0.6}Sr_{0.4}CoO_3$ nanoparticles were synthesized via a sol-gel chemical process and the physicochemical properties of these composites were characterized by X-ray diffraction (XRD), scanning electron microscopy (SEM), transmission electron microscopy (TEM), and energy-dispersive x-ray spectroscopy analysis (EDAX). Dielectric parameters were studied in a wide range of frequencies and temperatures. Further, these composites were evaluated for photodegradation activities towards MB dye under sunlight irradiation.

Key Words: $La_{1-x}Sr_xCoO_3$(LSCO), methylene blue (MB), oxygen evolution reaction (OER), photodegradation.

I. INTRODUCTION

Recently, water pollution with hazardous wastes and toxic water pollutants has been a great attention for the scientists. The wastewater from textile, paper, and other industries contain residual non-biodegradable dyes causing many serious problems to environment. Moreover, the residues of non-biodegradable dyes into the eco-system act as a source of esthetic pollution, eutrophication and perturbation in the aquatic life. Although various chemical and physical process is available for the degradation of textile effluents but they generate non-biodegradable contaminations and further require treatment involving expensive procedure. Conventional techniques such as coagulation/ flocculation, membrane separation, absorption methods as well as biological methods are also inefficient for removal of complex organic compounds [1- 8]. To resolve such types of problems Advanced Oxidation Processes (AOPs) are proven to be most promising technique which is based on the generation of highly reactive hydroxyl radicals (- OH) [9-17]. This is the most cost-effective chemical method which is extensively used for treatment of textile effluents and variety of organic pollutants [18-22]. Fast degradation of dye is achieved due to the high oxidative power of (- OH) radicals (2.83 V) and it can be further improved by using UV-visible radiations that generate additional hydroxyl radicals. The major advantages of the photocatalytic process are that there is no further requirement of secondary disposal methods and also not require expensive oxidizing chemicals.

Among various photo-catalytic materials, the metal oxide, perovskite type oxides, present themselves as one of the marvelous group of materials

with diverse and exotic properties such as the oxygen content in perovskite materials leads to high catalytic activity, doping of metal in desired amount is easily possible. Among these perovskites, the cobalt-based type $LaCoO_3$ perovskite ignited interest in the research since the early 1960s [23,24] and continues to be the material of the moment. $LaCoO_3$ perovskite has been shown to have promising catalytic activity for oxygen evolution reaction (OER) [25, 26]. Lanthanum, La, is a relatively large cation and gives structural stability to the catalyst. Rare-earth oxides with full or partially filled inner shells of lanthanide ions would involve the 4f electrons. The 4f electrons contribute to the density of states around the Fermi level, and degenerate strongly, the bandwidth is narrow and steep. The presence of La3+ with no 4f electrons is beneficial because the electrical conductivity increases and the effective mass decreases [27]. Cobalt, Co, cation, a transition metal with smaller size than La cation, is responsible for catalytic activity. In its compounds, cobalt nearly always exhibits a +2 or +3 oxidation state, although states +4, +1, 0, and −1 are also known [28]. Cobalt chemistry is dominated by the behavior of the 3d electrons. The outer electrons of the element are either in the 3d or 4s subshell. Oxidation state of Co helps the $LaCoO_3$ catalytic activity for OER which can be associated with Co3+ oxidation state. Co3+ active sites by absorption of −OH may act as reactants for OER [29].

In this study we report the effects on the structural and electrical phenomena caused by the doping of divalent (Sr2+) cations on LaCoO3 synthesized by the sol– gel method. Further, the as-synthesized nanocomposites were tested for their photocatalytic activities towards elimination of MB dye from aqueous solution under sun-light irradiation.

Experimental

Materials and Method

Nanocrystalline material with composition $La_{1-x}Sr_xCoO_3$ (x = 0.0, 0.4) (LSCO) were prepared by Sol-gel method. For the synthesis of this perovskite LSCO powder, all chemicals used were of analytical reagent (AR) grade and were used without further purification. At the beginning stoichiometric ratio of lanthanum nitrate La $(NO_3)_3{\cdot}6H_2O$, cobalt nitrate Co $(NO_3)_3{\cdot}6H_2O$, strontium nitrate Sr $(NO_3)_2$, and citric acid monohydrate $C_6H_8O_7.H_2O$ were weighted and dissolved in ethylene glycol $C_6H_6O_2$. Then the mixture was stirred magnetically at 80°C for 3h to get a homogeneous and transparent solution. The solution was further heated in a pressure vessel at about 130°C for 12h. During this reaction, a transparent solution was transformed into a gel state having very high viscosity. The material was then heated in a muffle furnace at 350°C for 3h and violet combustion occurs which spontaneously propagates until all the gel was burnt out to form into a loose powder and then milled to a fine powder. To improve the crystallinity of the precursor, the dried powder was then calcined in the range 550-750°C for 6h.

Result and discussion

X-ray diffraction analysis (XRD)

The structural properties of the prepared composites were characterized by X-ray diffraction. The XRD patterns for the synthesized $La_{1-x}Sr_xCoO_3$ (x = 0.0, 0.4) nanocomposites prepared by sol-gel method and calcined at 650°C are depicted in fig 1. The result obtained are in good agreement with XRD results previously reported in the literature [30]. From Figure 1 (curve A), it can be seen that all the diffraction peaks for pristine $LaCoO_3$ appearing at 23.24, 32.98, 42.53, 47.48, 57.34, 67.18 2θ can be induced to (012), (110), (202), (024), (018), (220) planes of the cubic structure of $LaCoO_3$ as per JDPDS card no. 24-1016. [31] From Figure 1 (curve B), the peak for (012), (104), (202), (024), (018), (220) plane appears at 23.24, 32.48, 42.53, 47.48, 57.34, 67.18 and experiences a slight shift of 0.5 2θ degrees which conform the doping of Sr^{2+} in $LaCoO_3$ host lattice. Further, in curve B, no impurity peak related to Sr^{2+} was observed which suggests the dissolution of $Sr2^+$ for this doping concentration. The ionic radii of Sr^{2+} (1.21 Å) are very close to that of La^{3+} and Sr is incorporated into the $LaCrO_3$ lattice at the La site. The crystallite size of $La_{1-x}Sr_xCoO_3$ (x=0, 0.4) powder was computed from the most intense peak of the XRD pattern using Scherrer's equation (Eq. 1)

$$D = 0.9\,\lambda/\beta\cos\theta \ldots\ldots\ldots (1)$$

where D is the crystallite size, λ refers to the wavelength of X-rays, β belongs to the full width at the half maxima value, and θ is considered as the Bragg's angle. According to the above equation, the calculated crystallite size of $La_{1-x}Sr_xCoO_3$ (x=0, 0.4) was found to be in the range of 30–35 nm.

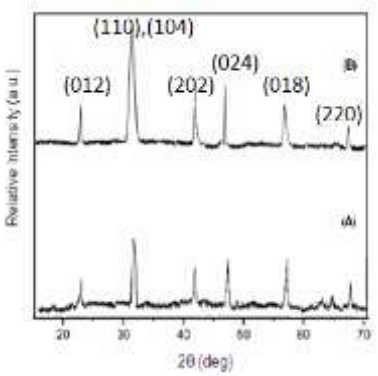

Fig1: XRD spectra of (A) $LaCoO_3$ (B) $La_{0.6}Sr_{0.4}CoO_3$ calcined at 650ºC

Transmission electron microscopy analysis (TEM)

The nanostructure of the typical sample was analyzed by using Transmission Electron Microscope (Philips CM 20). The TEM images of representative nanocrystalline $La_{06}Sr_{0.4}CoO_3$ calcinated at 650ºC are as shown in Figure 2. TEM analysis revealed that the particles are nearly spherical. The average particle size as determined from TEM is 30 nm is found to be in close agreement with that obtained from XRD studies. TEM analysis of the sample revealed the polycrystalline nature of the sample

.

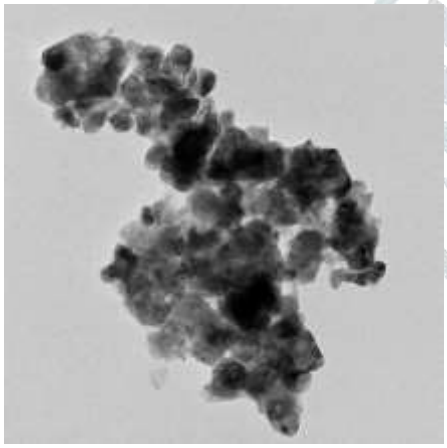

Fig2: TEM of $La_{0.6}Sr_{0.4}CoO_3$ calcined at 650ºC

Surface Morphology

In order to study particle size and surface morphology scanning electron microscopy was performed. From the SEM images of pristine $LaCoO_3$(Figure 3. A and B), it was seen that the sample exhibits spherical morphology. The spherical nanomaterial has uniformly grown and homogeneously distributed leading to a generation of voids which might give a reasonable high surface area. SEM images of representative $La_{0.6}Sr_{0.4}CoO_3$ sample are depicted in (Figure4. C and D). From Figure, it also exhibits a similar morphology as that of the undoped $LaCoO_3$ sample. However, a closure observation reflects that doping $LaCoO_3$ with Sr^{2+} has led to an agglomeration of spherical units to some extent.

The particle size of both the samples as evaluated using Image J software was found to be in the range of 30-35nm. This is very well in agreement with those of the XRD
results.

Energy dispersive x-ray spectroscopy analysis (EDX)

To examine the chemical composition, EDX has been carried out and the EDX spectrum is as shown in Fig. 5. The EDX analysis showed the presence of La, Co, Sr, and oxygen without any impurity.

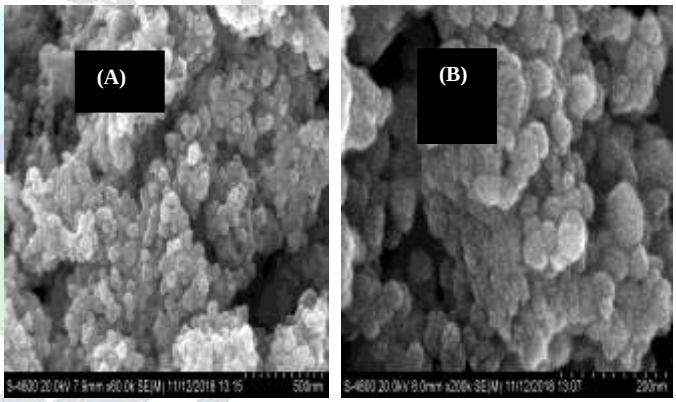

Fig. 3: SEM micrograph of pristine Nanocomposites $LaCoO_3$

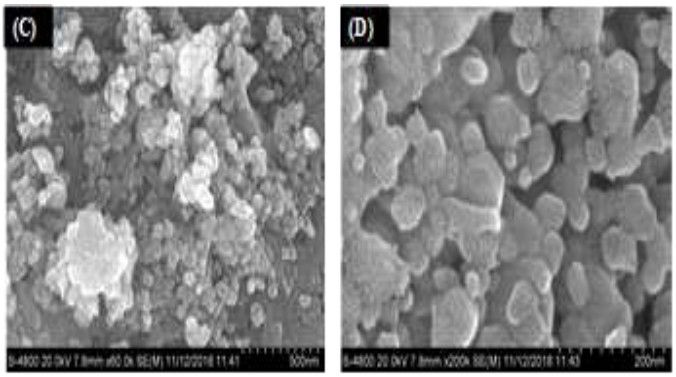

Fig. 4: SEM micrograph of $La_{0.6}Sr_{0.4}CoO_3$ Nanocomposites

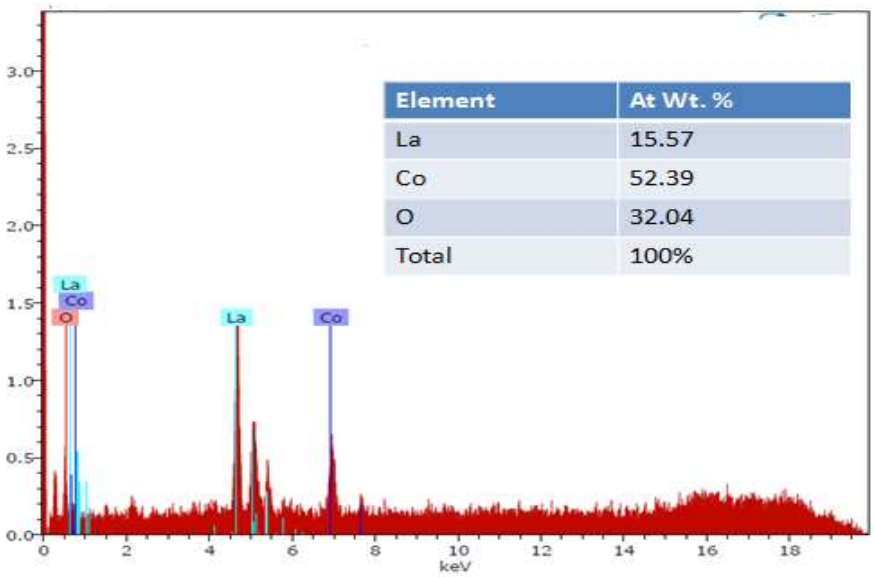

Fig.5 EDX spectrum of Sr substituted $LaCoO_3$ perovskites

.

Dielectric study

Dielectric behavior is an important property of materials and it depends on the particle size, method of formation, sintering temperature, and composition of materials [32] The dielectric study of $LaCoO_3$ and $La_{0.6}S_{r0.4}CoO_3$ was done using Hi Tester (HIOKI 3522-50) LCR meter in the frequency range 42Hz to 500KHz from room temperature (RT) to 700°C. The dielectric constant or relative permittivity (ε′) is the ratio of the permittivity of a substance to the permittivity of free space. The dielectric constant is the measure of the polarity of a medium

[33]. The dielectric constant (ε′) and dielectric loss (ε″) were calculated using the formulas

$$\varepsilon' = cd/\varepsilon_0 A$$

$$\varepsilon'' = \tan\delta\ \varepsilon'$$

Where C is the measured capacitance of the sample, d is the thickness of the sample, A is the area of the sample.

Figure 6(a, b) shows the frequency dependence of dielectric constant ε' at different temperatures for the compositions $La_{1x}Sr_xCoO3$ (x= 0, 0.4,)) calcined at 550°C. It is clear from the figure that ε' decreases with frequency and increases with temperature. The decrease of ε' with frequency can be attributed to the fact that at low frequencies ε' polar material is explained by the the contribution of multicomponent of polarizability, deformational (electronic and ionic), and relaxation (orientation and interfacial) polarization. First, electronic polarization arises from the displacement of the valence electrons relative to the positive nucleus. This type of polarization takes place at frequencies up to 1016Hz. The second type is ionic polarization, which occurs due to the displacement of negative and positive ions with respect to each other. The maximum frequency of ionic polarization is 1013 Hz. Third, dipolar polarization occurs if the material contains molecules, with a permanent electric dipole moment that can change orientation into the direction of the applied electric field. The dipolar polarization takes place at frequencies up to 1010 Hz. The final one is the space charge polarization which occurs due to the impedance of mobile charge carriers by interfaces. Space charge polarization typically occurs at a frequency range from 1 to 103 Hz. The total polarization of the dielectric material can be given as the sum of these four types of polarization [34]. The obtained results in the present study may be referred to as the total polarization. When the frequency is increased, the orientational polarization decreases since it takes more time

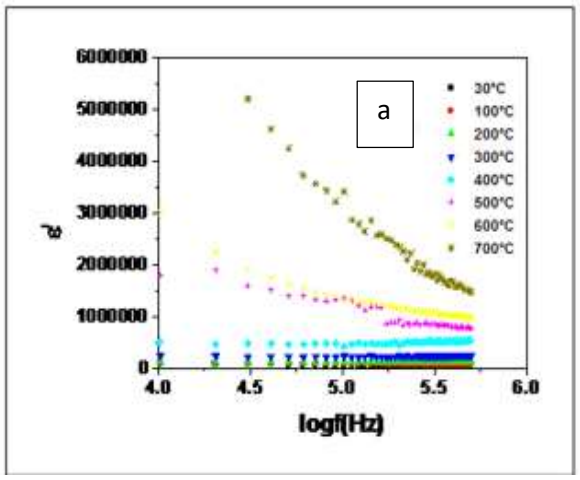

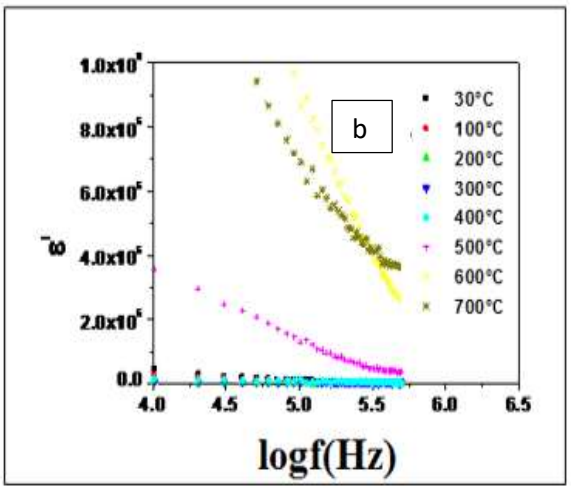

Fig 6(a, b). Frequency and temperature dependence of the dielectric constant (ε') of sample a) $LaCoO_3$ b) $La_{0.6}Sr_{0.4}CoO_3$

than electronic and ionic polarization. This decreases the value of dielectric constant ε' reaching a constant value at a higher frequency correspondingly to interfacial polarization. Figure 6(a,b)shows the temperature dependence of the dielectric constant *ε'* for the compositions $La_{1-x}Sr_xCoO_3$(x= 0, 0.4,) calcined at 550°C respectively It is clear from the figure that *ε'* increases with temperature. The increase of *ε'* with temperature can be attributed to the fact that the orientational polarization is connected with the thermal motion of molecules, so dipoles cannot orient themselves at low temperatures. When the temperature has increased the orientation of the dipole is facilitated and this increases the value of orientational polarization, which leads to an increase in the dielectric constant ε' with temperature. The increase in *ε'* is also due to the increase in the degree of crystallinity [35-37].

Photocatalytic activity of La1-xSrxCoO3 (x=0.0, 0.4)

The Photocatalytic performance of as-synthesized (undoped and 0.4% Sr doped $LaCoO_3$) samples was studied using methylene blue (MB) dye as a degradation under sunlight. To monitor the degradation process UV–Visible spectrophotometer was used. To achieve adsorption-desorption equilibrium, dye solution containing photocatalyst was kept in dark for 30 mins before photocatalytic degradation. The degradation experiments were performed under natural sunlight irradiation. The samples were analyzed using a UV-visible spectrophotometer after a repeated interval of 15 mins during the experiment.

The pseudo-first-order rate kinetics was followed for photocatalytic degradation of MB dye and rate constant value was determined by the following relation;

$$\ln\left(\frac{C^0}{C}\right) = kt$$

Where the k value was calculated from the graph between $\ln\left(\frac{C^0}{C}\right)$ versus time interval, C denote the M.B dye concentration at t = 0 and t = t respectively.

For the degradation of Methylene blue (MB) dye under sunlight irradiation, the photocatalytic activities of the as-prepared $La_{1-x}Sr_xCoO_3$ (x= 0,0.4) were evaluated. In terms of the efficiency of decolorization, the photodegradation process was evaluated while the photocatalytic activity was controlled using 662 nm as the peak of optical absorption. Photodegradation of MB dye with an initial concentration of 10 ppm due to the irradiation period is as shown in Figure 8.a. The intensities of the signature absorption peaks can be observed to decrease with an increase in time. That indicates the photocatalyst's progressive degradation of MB dye.

Figure (8b) shows the absorption of adsorbed and degraded MB dye in the presence of $La_{1-x}Sr_xCoO3$(x= 0,0.4) under specific experimental conditions at different periods. In addition, for comparison, a controlled experiment without any catalyst was also conducted. In the absence of a

catalyst, MB dye was barely degraded, but MB dye degradation was noted in the presence of a catalyst under sunlight irradiation.

Figure 8. b shows that undoped $LaCoO_3$ displayed a lower degradation rate of MB relative to cobalt-doped ferrites. The photodegradation rate of MB dye was observed to be $La_{0.6}Sr_{0.4}CoO_3$ > LaCoO3. This pattern demonstrates clearly that with the rise in Sr2+, deterioration increases. Of all, under sunlight irradiation, $La_{0.6}Sr_{0.4}CoO_3$ displayed the highest rate of photodegradation. Furthermore, for the determination of reaction kinetics, experimental data is used.

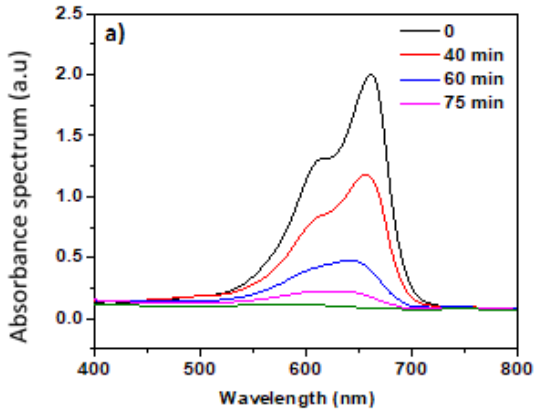

Figure 8. (a) Spectral changes during the degradation of MB dye in the presence of $La_{0.6}Sr_{0.4}CoO_3$

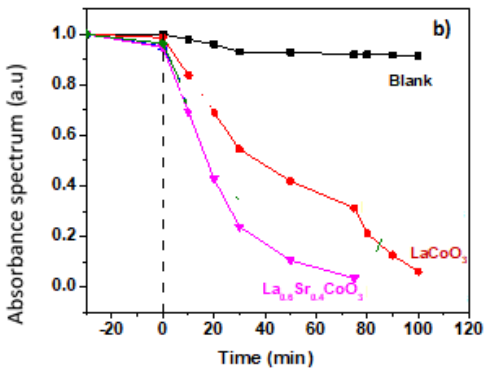

Fig.8 (b) A plot of the change in absorbance vs. irradiation time in the presence of the different $La_{1-x}Sr_xCoO3$ catalysts

The rate constants of $LaCoO_3$ and $La_{0.6}Sr_{0.4}CoO_3$ were found to be 0.052 and 0.084 min-1 respectively. Thus, with excellent linear
correlation suggesting pseudo-first-order kinetics, $La_{0.6}Sr_{0.4}CoO_3$ has demonstrated high photodegradation speeds. $La_{0.6}Sr_{0.4}CoO_3$ shows maximum MB considering the strong spectral response to sunlight and is due to the reduction of the $La_{1-x}Sr_xCoO_3$ band difference. The bandgap of samples is well within the visible region, so it will consume the maximum amount of sunlight, creating the highest number of electron-hole pairs.

Conclusion: $LaCoO_3$ and $La_{0.6}Sr_{0.4}CoO_3$ nanomaterials were successfully synthesized by sol–gel method with the citric acid as a chelating agent in the ethylene glycol solution and utilized as photocatalysts for the degradation of MB dye. Both XRD and SEM analysis revealed the particle size of as synthesized samples in the range of 30-35nm. Both the dielectric constant **ε'** and dielectric loss **ε''** increased with temperature and decrease with frequency through the studied ranges. The temperature dependence of the dielectric loss was expected to be associated with the conduction loss. The photodegradation rate of MB dye observed to be greater for $La_{0.6}Sr_{0.4}CoO_3$ than for LaCoO3. This pattern demonstrates clearly that with the doping of Sr2+, deterioration increases. Of all, under sunlight irradiation, $La_{0.6}Sr_{0.4}CoO_3$ displayed the highest rate of photodegradation.

REFERENCES:

[1] C. O. Neil, A. Lopez., S. Esteves, F. R. Hawkes, D. L. Hawkes, S. Wilcox, *Appl. Microbiol. Biotechol.*, 53, 249(1999)

[2] N. Nasuha, B. H. Hameed, A. T. M. Din, *J. Hazard. Mater*., 175 ,126 (2010)

[3] M. A. Rauf, S. M. Qadri, S. Ashraf, K. M. Al-Mansoori, *Chem. Eng. J*., 150, 90(2009)

[4] L. Ahmad, S.W. Puasa, *Chem. Eng. J*., 132, 257 (2007).

[5] K. Shakir, A. F. Elkafrawy, H. F. Ghoneimy, S. G. Elrab Beheir, M. Refaat, *Water Res.*, 44, 1449(2010).

[6] M. S. Lee, C. Huang, K. R. Lee, J. R. Pan, W. K. Chang, *Desalination*, 234, 416 (2008).

[7] H. Jirankova, J. Mrazek, P. Dolecek, J. Cak, *Desalination and Water Treat*., 20, 96 (2010) .

[8] M. A. Rauf and S. S. Ashraf, *Dyes and Pigments: New Research, Nova Science Publishers*, Inc. (ISBN: 978-1-60692-027-5) (2009)

[9] L.Ayed, K. Chaieb, A. Cheref, A. Bakhrouf, *Desalination*, 260, 137 (2010).

[10]O. Cinar, S. Yasar, M. Kertmen, K. Demiröz, N.O. Yigit, M. Kitis, *Process Safety Environ. Protect*., 86, 455(2008).

[11] P. A. Soares , T. F. Silva , D. R. Manenti , S. M. Souza , R. A. Boaventura , V. J. Vilar, *Environ Sci Pollut Res Int*., 21, 932 (2014) .

[12] Masarwa, S. Rachmilovich-Calis, N. Meyerstein, D. Meyerstein, *Coord. Chem. Reviews.*, 249, 1937 (2005).

[13]J. M. Monteagudo, A. Duran, I. S. Martin, M. Aguirre, *Appl. Catalysis B: Environ*. 95, 120 (2010)

[14] N. Modirshahla, M. A. Behnajady, F. Ghanbary, *Dyes and Pigments*, 73, 305 (2007)

[15] M. A. Rauf, M. A. Meetani, A. Khaleel, A. Ahmed, *Chem. Eng. J*., 157, 373 (2010).

[16] Balcioglu, Akmehmet, I. Arslan, *Environ. Pollution*., 103 , 261 (1998)

[17] C. P. Huang, C. Dong, Z. Tang, *Waste Management*., 13, 361 (1993) .

[18] N. N. Mahamuni, Y. G. Adewuyi, *Ultrasonics Sonochem.*, 17, 990 (2010)

[19] D. P. Mohapatra, S. K. Brar, R. D.Tyagi, P. Picard,R. Y. Surampalli, *Sci. Total Environ.*,470–471, 58 (2014).

[20] M. H. Pérez, G. Peñuela, M. I. Maldonado, *Appl. Catal. B. Environ*., 64, 272 (2006).

[21] M. Pera-Titus, V. García-Molina, M. A. Baños, J. Giménez, S. Esplugas, *Appl. Catal. B. Environ*., 47, 219 (2004) .

[22] C. Bouasla, M. E. H. Samar, F. Ismail, *Desalination*, 254, 35 (2010).

[23] Heikes R, Miller RC, Mazelsky R. *Physica. 1*964;30(8):1600-1608. DOI: 10.1016/0031-8914(64)90182-X

[24] Menyuk N, Dwigh K, Raccah PM. *Journal of Physics and Chemistry of Solids.* 1964;28(4):549-556. DOI: 10.1016/0022-3697(67)90085-6

[25] Enache S, Dragan M, Soare A, Ebrasu DI, Zaulet A, Varlam M, et al.*Special Issue of Bulgarian Chemical Communications, Sofia, Bulgaria.* 2018;50(A):127-132

[26] Ebrasu DI, Zaulet A, Enache S, Dragan M, Carcadea E, Varlam M, et al. *Special Issue of Bulgarian Chemical Communications, Sofia, Bulgaria.* 2018;50(A):133-138

[27] Cullity BD, Graham CD. *Introduction to Magnetic Materials. 2nd ed. Hoboken, New Jersey, United States: Wiley-IEEE Press*; 2008. 171p. DOI: 10.1002/9780470386323

[28] NN, Earnshaw A, editors. *Chemistry of the Elements. 2nd ed. Oxford, United Kingdom: Butterworth-Heinemann*; 1997. 1113p. DOI: 10.1016/ B978-0-7506-3365-9.50032-8

[29] Zhu H, Zhang P, Dai S. *Catalysis.* 2015;5(11):6370-6385. DOI: 10.1021/acscatal.5b01667

[30] X.Ding, Y.Liu,L.Gao and L.Guo, ,*Journal of Alloys and Compounds*, Vol. 458, No. 1-2, (2008), 346- 350.

[31] M.M. Fukate, A.B. Bodade, G.N. Chaudahry, *Nano Trends*, 19(3) (2017) 49-55

[32] Ali R, Khan MA, Mahmood A, Chughtai AH, Sultan A, Shahid M, *Ceram Int* 2014; 40:3841–6.

[33] Nawaz S, Malik H, Warsi MF, Shahid M, Shakir I, Wadood A, etal..*Ceram Int* 2015;41:6812–6.

[34] M. Barsoum, *Fundamentals of Ceramics, Mc Graw--Hill*, New York (1977) 543.

[35] W. Cao, R. Gerhardt, *Solid State Ion.* 42 (1990) 213

[36]T.G. Abdel-Malak, M.E. Kassem, N.S. Aly, S.M. Kalil, *Acta Phys. Pol.* A 81 (1992) 675

[37] R. Singh, R.P. Tandon, V.S. Panwar, S. Chandra, *J. Appl. Phys.* ,69 (1991).2504